Single-transistor method for the extraction of the contact and channel resistances in organic field-effect transistors

DOI:
10.1063/1.4868042

Single-transistor method for the extraction of the contact and channel resistances in organic field-effect transistors

Fabrizio Torricelli,[1, a)] Matteo Ghittorelli,[1] Luigi Colalongo,[1] and Zsolt Miklos Kovacs-Vajna[1]
Department of Information Engineering, University of Brescia, via Branze 38, 25123 Brescia, Italy

(Dated: 13 January 2014)

A simple and accurate method for the extraction of the contact and channel resistances in organic field-effect transistors (OFETs) is proposed. The method is of general applicability since only two measured output-characteristics of a single OFET are needed and no channel-length scaling is required. The effectiveness of the method is demonstrated by means of both numerical simulations and experimental data of OFETs. Furthermore, the provided analysis quantitatively shows that the contact resistance in OFETs depends on both V_G and V_D, and, in the case of non-linear injecting contact, the drain-source voltage (viz. the electric field along the channel transport direction) plays a major role.

The performance of organic field-effect transistors (OFETs) is strictly connected to the charge injection from the source electrode into the organic semiconductor and to the charge transport in the channel accumulated at the gate-insulator/organic-semiconductor (OSC) interface. In the last years, the improvement of both holes and electrons mobility has been impressive. State-of-art single crystal OSCs yields OFETs with an average field-effect mobility as high as[1] 16.4 cm^2/Vs. Even in the case of fully-printed low-temperature complementary organic technologies, the p- and n-type OFETs show mobilities up to[2] 1.5 cm^2/Vs.

Charge injection is currently limiting the performance of organic field-effect transistors (OFETs). It restricts, and in some cases nullifies, the benefits of high-mobility organic semiconductors (OSCs) hampering the channel-length scaling[3,4]. Poor charge injection results in a large contact resistance eventually leading to OFETs with reduced drive current and operating frequency, small on/off current ratio, and large threshold voltage[4,5]. The aforementioned parameters are of paramount importance to achieve organic circuits operating at low supply voltage, and with a large level of integration and functionalities. To further improve the OFET technology, it is essential to disentangle and quantify the contact and channel resistances directly from the measured electrical characteristics.

To this aim, standard techniques like four-probe measurements[6–8] and transfer-line method (TLM)[9–13] have been widely used. The main shortcoming is that the former require complex electrode patterning applicable only to laboratory devices; while the latter requires several nominally identical transistors with scaled channel lengths. Since organic technologies suffer from large variability and modest stability, a method able to extract the contact R_p and channel R_{ch} resistances directly from a single OFET is highly desirable. In the case of linear-injecting contacts, the transition-voltage method[14] provides a good estimation of the contact resistance making use of the transfer and output characteristics of a single transistor. In the case of non-linear injection, which is observed in high-mobility[1,15] or short-channel OFETs[3,4], the accurate extraction of R_p and R_{ch} without the need of channel-length scaling is still an open issue.

In this letter we propose a simple and accurate method able to provide both the contact and channel resistances of OFETs with non-linear injecting contact. The method requires the measurements of only two output characteristics of a single transistor without the need of transistor scaling. We call it Single-Transistor Method (STM).

A general approach to analyze the contact is to split the channel into a small contact region, where there is a voltage drop V_C, and the main channel, where the voltage drop is $V_D - V_C$[16,17]. This is schematically illustrated in Fig. 1. The contact region is spatially located at the source side of the OFET, since most of V_C drops at the injecting electrode[18–20]. The drain current I_D as a function of gate V_G, drain V_D, and source V_S voltages is given by[21,22]

$$I_D = \beta \left({\Psi_S}^{\gamma} - {\Psi_D}^{\gamma} \right) \tag{1}$$

where β is a prefactor dependent on geometrical and physical parameters, γ accounts for the OSC energetic disorder, Ψ_S and Ψ_D are proportional to the accumulated charges per unit area at the source and drain, respectively, $\Psi_S = V_G - V_{th} - V_{S'}$, $\Psi_D = V_G - V_{th} - V_D$. V_{th} is the threshold voltage, and $V_{S'} = V_S + V_C$ is the virtual source potential (i.e. the channel potential at the source side). In case of no contact resistance: $V_{S'} = V_S$.

It was shown that the contact resistance depends on the Schottky barrier Φ_B due to the energy misalignment between the OSC and the metal electrode[23,24], on the quality of the OSC close to the metal edge[18,25], and on the local electric fields[19]. Hence, the contact voltage drop V_C is modeled as (Fig. 1)

$$V_C = R_s \times I_D + V_{inj} \tag{2}$$

where R_s accounts for the parasitic resistance due to the OSC quality close to the contact, and V_{inj} is the contact potential required for injection.

a) Electronic mail: fabrizio.torricelli@ing.unibs.it.

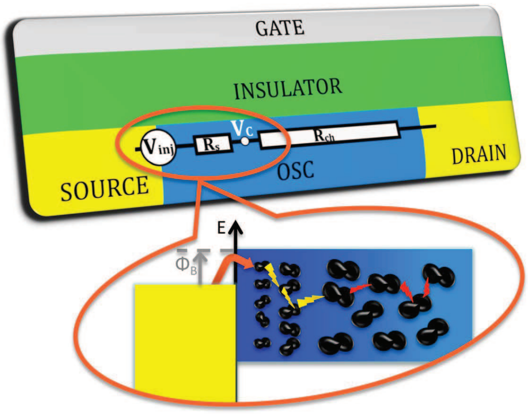

FIG. 1. Cross-section of an OFET. R_{ch} is the main channel resistance, while the contact resistance accounts for metal-organic injection (V_{inj}) and charge transport in the low-quality region close to the contact (R_s). Zoom: schematic illustration of the injection, transport in the low-quality OSC and transport in the OSC channel region.

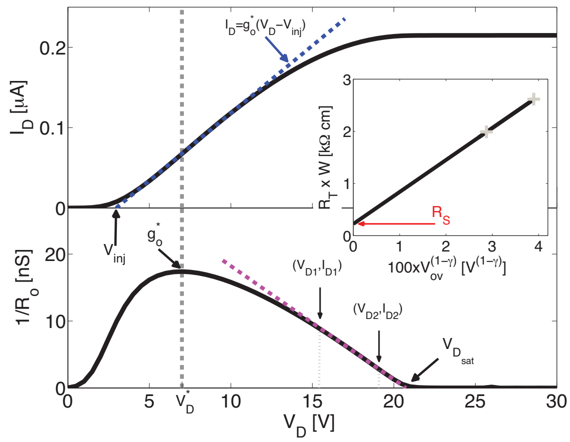

FIG. 2. Typical output characteristic (top panel) and transconductance (bottom panel) of an OFET with a large non-linear contact resistance; data are taken from[20]. Inset: Normalized total resistance R_T as a function of $100\times {V_{ov}}^{(1-\gamma)}$. The resistance is normalized by the transistor width W.

In the following, the idea is to calculate the contact and channel parameters (namely R_s, V_{inj}, β, γ, V_{th} in Eqs. 1-2) by means of only two output characteristics measured at two different values of V_G. Once the "intrinsic" channel parameters are determined (viz. β, γ, and V_{th}), R_{ch} is given by Eq. 1 calculated at $V_S = V_{S'}$ and it reads:

$$R_{ch} = \left[\frac{\partial I_D^{Eq.1}}{\partial V_D}\right]^{-1}_{V_S=V_{S'}} = \frac{1}{\beta\gamma {\Psi_D}^{\gamma-1}} \qquad (3)$$

and the overall contact resistance results:

$$R_p = R_o - R_{ch} \qquad (4)$$

where $R_o = (\partial I_D/\partial V_D)^{-1}$ is the measured output resistance. It is worth noting that the contact model (Eq. 2) is not used to directly calculate the contact resistance but only to obtain the channel parameters. This is the key point to keep both the contact model simple and the extraction procedure accurate.

Typical output characteristics and conductances measured for OFETs with non-linear injecting contacts are shown in Fig. 2. The effect of the contact resistance is readily visible in the S-shape of the $I_D - V_D$ curve and in the non-monotonic behavior of the output conductance $g_o = 1/R_o$.

At small values of V_D ($V_D < V_{inj}$), g_o strongly increases: the current is injection-limited and it is enhanced by the longitudinal electric field (viz. V_D). When $V_D = V_{inj}$, the drain current $I_D \simeq 0$, the measured total resistance is $R_T = R_o(V_{inj})$ and it reads:

$$R_T = \left[\frac{\partial I_D}{\partial V_D}\right|^{-1}_{V_D=V_{inj}} = \frac{1}{\beta\gamma}{V_{ov}}^{(1-\gamma)} + R_s \qquad (5)$$

where $V_{ov} = V_G - V_{th} - V_{inj}$. The inset of Fig. 2 shows the measured R_T as a function of ${V_{ov}}^{(1-\gamma)}$. At least two $I_D - V_D$ characteristics measured at different V_G voltages are required. According to Eq. 5, the intercept to the y-axis gives R_s.

When $V_D > V_{inj}$ the drain current linearly increases with V_D thus indicating that the injection process becomes rather efficient and the source contact supplies enough carriers for the channel transport. The output conductance has a maximum g_o^* at $V_D = {V_D}^*$, and in this region the drain current $I_D = g_o^*(V_D - V_{inj})$ (Fig. 2), which gives:

$$V_{inj} = {V_D}^* - {I_D}^*/{g_o}^* \qquad (6)$$

where ${I_D}^*$ is the measured I_D at $V_D = {V_D}^*$. V_{inj} is the crossing point between the x-axis and the linear fit of I_D around the point ${I_D}^* - {V_D}^*$ (top panel of Fig. 2).

When the drain voltage is larger than ${V_D}^*$ (${V_D}^* < V_D < V_{D_{sat}}$), g_o monotonically decreases: the current is limited by the charge transport in the OFET channel, and the measured output resistance is $R_o \simeq R_s + R_{ch} = R_s + 1/[\beta\gamma {\Psi_D}^{(\gamma-1)}]$. By equating the R_o values obtained at two different V_D (V_{D1} and V_{D2} in the bottom panel of Fig. 2), the OSC disorder parameter is calculated:

$$\gamma = 1 + \ln\left[\frac{R_o(V_{D2}) - R_s}{R_o(V_{D1}) - R_s}\right] \Big/ \ln\left[\frac{\Psi_{D1}}{\Psi_{D2}}\right] \qquad (7)$$

When the OFET is approaching the saturation voltage $V_{D_{sat}}$ the output conductance ideally goes to zero. At $V_D = V_{D_{sat}}$ the OFET channel is pinched-off, and the threshold voltage parameter reads:

$$V_{th} = V_G - V_{D1} + \frac{g_o(V_{D1})}{g_o(V_{D2}) - g_o(V_{D1})}(V_{D2} - V_{D1}) \qquad (8)$$

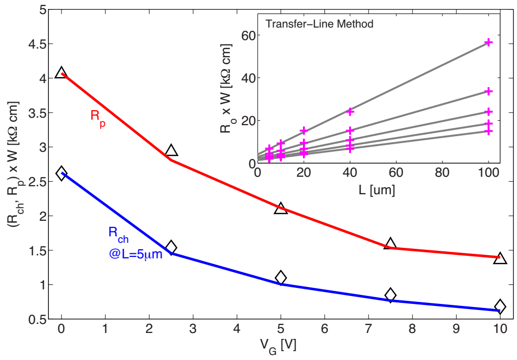

FIG. 3. Main panel: channel and contact resistances as a function of the gate voltage. Symbols are calculated with the TLM and lines with the STM. Inset: overall OFET resistance as a function of the transistor length ($L = 100, 40, 20, 10, 5\ \mu m$). R_o is calculated at $V_D = 0.1V$. The OFETs are bottom-gate bottom-contact, the OSC is pentacene, the gate insulator is aluminum oxide and the electrodes are gold. The measurements and the OFETs fabrication are reported in Refs.[26,27].

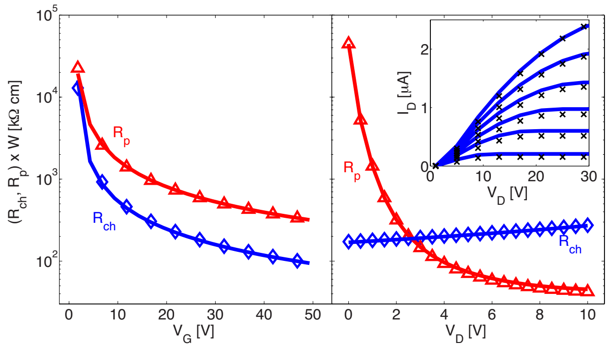

FIG. 4. Contact (triangles) and channel (diamonds) resistances as a function of gate (left panel, $V_D = 2\ V$) and drain (right panel, $V_G = 25\ V$) voltages. Data are taken from[28], and resistance values are calculated with the model and parameters of[20]. Lines are calculated with the proposed method. Inset: output characteristics as a function V_G ($V_G = 20 \rightarrow 40\ V$, step of $5\ V$). Data (symbols) are taken from[28], lines are calculated with Eqs. 1-2.

Hence, given an $I_D - V_D$ curve, the parameters V_{inj}, γ, and V_{th}, are obtained using Eqs. 6, 7, and 8, respectively. γ is firstly calculated assuming $R_s = 0$ in Eq. 7, and it is used as an initial value. As a second step, another output curve is measured and R_s is calculated according to Eq. 5. Then, R_s is plugged into Eq. 7 and a new value of γ is obtained. Since the OFET operating conditions guarantee that in Eq. 7 $R_o >> R_s$, only few iterations of Eqs. 5, and 7 are required. Finally, by observing that at $V_D = {V_D}^*$ the maximum of the output conductance can be written as $g_o^* = \beta\gamma\Psi_{D*}^{\gamma-1}/(1+\beta\gamma R_s \Psi_S^{\gamma-1})$, the parameter β reads:

$$\beta = \left\{ \frac{\gamma}{g_o^*} \left[{\psi_{D*}}^{(\gamma-1)} - g_o^* R_S {\psi_S}^{(\gamma-1)} \right] \right\}^{-1} \tag{9}$$

The contact and channel resistances determined with the proposed method (STM) and the widely used TLM are shown in Fig. 3. There is a very good agreement between the two methods in the whole range of gate voltages. It is worth noting that OFETs with different channel lengths are required by the TLM (inset of Fig. 3) while the STM enables to calculate R_p and R_{ch} with only one OFET.

In order to assess the accuracy of the proposed method, the "exact" contact and channel resistances calculated with the numerical model proposed in[20] are compared to the values given by the STM in Fig. 4. The numerical model[20] is taken as a benchmark because it accounts for both charge injection and transport in OFETs and it accurately reproduces the measurements reported in[20,28]. The results show a very good agreement in the whole range of gate and drain voltages. As expected, increasing V_G both R_{ch} and R_p get smaller (Fig. 4, left panel). The lowering of the contact resistance with V_G is commonly observed in contact-limited OFETs and it is explained by trap-filling[14], Schottky-gated injection[16], and spatial modulation of the contact region[19].

R_{ch} and R_p show an opposite dependence on the drain voltage (Fig. 4, right panel). R_{ch} increases with V_D because the transistor is moving towards the saturation; while R_p decreases since the injection process is enhanced by the electric field. R_{ch} and R_p as a function of both V_G and V_D are shown in Fig. 5. Independently of the gate voltage, at $V_D \simeq 3V$ results that $R_{ch} = R_p$. We also found that the transition voltage from contact-limited to channel-limited current corresponds to the injection voltage V_{inj} and it increases at larger Schottky barriers. This behavior can be explained as follows. A depleted region in the OSC close to the source electrode is formed because of the metal-organic energy misalignment. Since the transistor is a bottom-gate bottom-contact architecture, the width of the depleted region is basically independent of the barrier height Φ_B and hence the drain voltage enhances the charge injection by lowering Φ_B. Increasing the barrier height, larger V_D is required to turn the non-linear injecting contact into an ohmic-like contact such that $R_p < R_{ch}$. Such a behavior suggests that a strongly contact-limited OFET biased at large V_G and $V_D < V_{inj}$ could be the ideal condition to assess the metal-organic contact properties.

In the light of the previous analysis, we can conclude that at small drain voltages ($V_D \leq V_{inj}$) the current is severely contact limited, while for $V_D \geq {V_D}^*$ the channel resistance is dominant compared to the contact resistance, and $R_o(V_D^*) \simeq R_{ch}(0)$. Hence, the presented method can be further simplified and the contact and channel resistances can be extracted directly from a single output characteristic (inset of Fig. 6): when V_D is small (i.e. $V_D < V_{inj}$) the overall resistance is $R_o = 1/g_o(0) = R_p + R_{ch}$, $R_{ch} \simeq 1/g_o^*$, and $R_p = R_o - R_{ch} = 1/g_o(0) - 1/g_o^*$. Fig. 6 shows a good

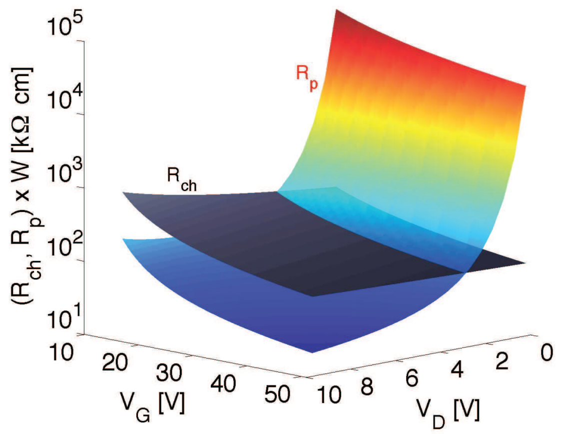

FIG. 5. Contact (color surface) and channel (black surface) resistances as function of gate and drain voltages calculated with the STM. The OFET parameters and the numerical model used for current calculations are reported in[20].

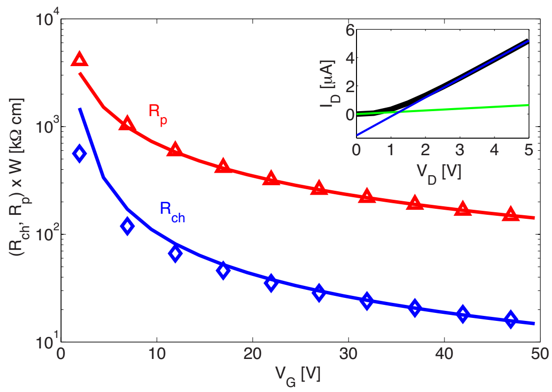

FIG. 6. Main panel: contact (triangles) and channel (diamonds) resistances calculated with the numerical model[20]. The OFET parameters are the same of Fig. 4, except for $\Phi_B = 0.45\ eV$. Lines are calculated with the simplified STM. Inset: (black line) output characteristic at $V_G = 50\ V$, (blue line) linear fit at $V_D = V_D^*$, (green line) linear fit at $V_D = 0.01\ V$.

agreement between R_p and R_{ch} obtained with the simplified STM (lines) and the exact values given by[20] (symbols). The channel resistance is slightly overestimated when $V_G < 10V$ because when V_D^* is close to V_G, comes that $R_{ch}(V_D^*) > R_{ch}(0)$.

In conclusion, the proposed STM method enables to determine both the contact and channel resistances as a function of V_G and V_D by means of only two measured output characteristics of a single transistor. It is simple, accurate, and of general applicability. Furthermore, a simplified version of the STM that requires only one output characteristic to estimate R_p and R_{ch} as a function of V_G is proposed and validated. The provided analysis shows that the contact resistance in OFETs with non-linear injecting contacts depends on both V_G and V_D, and the drain voltage plays a major role in the charge injection process. The presented approach is general and can be applied to any transistor technology where non-linear injection takes place, as for example zinc-oxide transistors[29].

[1] H. Minemawari, T. Yamada, H. Matsui, J. Tsutsumi, S. Haas, R. Chiba, R. Kumai, and T. Hasegawa, *Nature* **475**, 364 (2011).

[2] S. Jacob, S. Abdinia, M. Benwadih, J. Bablet, I. Chartier, R. Gwoziecki, E. Cantatore, A.H.M. van Roermund, L. Maddiona, F. Tramontana, G. Maiellaro, L. Mariucci, M. Rapisarda, G. Palmisano, and R. Coppard, *Solid-State Electron.* **84**, 167 (2013).

[3] F. Ante, D. Kälblein, U. Zschieschang, T. W. Canzler, A. Werner, K. Takimiya, M. Ikeda, T. Sekitani, T. Someya, and H. Klauk, *Small* **7**, 1186 (2011).

[4] F. Ante, D. Kälblein, T. Zaki, U. Zschieschang, K. Takimiya, M. Ikeda, T. Sekitani, T. Someya, J. N. Burghartz, K. Kern, and H. Klauk, *Small* **8**, 73 (2012).

[5] L. Giraudet, and O. Simonetti, *Org. Electron.* **14**, 219 (2011).

[6] R. J. Chesterfield, J. C. McKeen, C. R. Newman, and C. D. Frisbie, *J. Appl. Phys.* **95**, 6396 (2004).

[7] P. V. Pesavento, R. J. Chesterfield, C. R. Newman, and C. Daniel Frisbie, *J. Appl. Phys.* **96**, 7312 (2004).

[8] T. J. Richards, and H. Sirringhaus, *J. Appl. Phys.* **102**, 094510 (2007).

[9] D. J. Gundlach, L. Zhou, J. A. Nichols, T. N. Jackson, P. V. Necliudov, and M. S. Shur, *J. Appl. Phys.* **100**, 024509(2006).

[10] T. Minari, T. Miyadera, K. Tsukagoshi, Y. Aoyagi, and H. Ito, *Appl. Phys. Lett.* **91**, 053508 (2007).

[11] M. Kitamura, S. Aomori, J. Ho Na, and Y. Arakawa, *Appl. Phys. Lett.* **93**, 033313 (2008).

[12] Y. Xu, R. Gwoziecki, I. Chartier, R. Coppard, F. Balestra, and G. Ghibaudo, *Appl. Phys. Lett.* **97**, 063302 (2010).

[13] M. Imakawa, K. Sawabe, Y. Yomogida, Y. Iwasa, and T. Takenobu, *Appl. Phys. Lett.* **99**, 0233301 (2011).

[14] S. D. Wang, Y. Yan, and K. Tsukagoshi, *IEEE Electron Device Lett.* **31**, 509 (2010).

[15] S. Georgakopoulos, Y. Gu, M. M. Nielsen and M. Shkunov, *Appl. Phys. Lett.* **101**, 213305 (2012).

[16] A. Valletta, A. Daami, M. Benwadih, R. Coppard, G. Fortunato, M. Rapisarda, F. Torricelli, and L. Mariucci, *Appl. Phys. Lett.* **99**, 233309 (2011).

[17] R. A. Street, and A. Salleo, *Appl. Phys. Lett.* **81**, 2887 (2002).

[18] J. A. Nichols, D. J. Gundlach, and T. N. Jackson, *Appl. Phys. Lett.* **83**, 2366 (2003).

[19] J. J. Brondijk, F. Torricelli, E. C. P. Smits, P. W. M. Blom, and D. M. de Leeuw, *Org. Electronics* **13**, 1526 (2012).

[20] O. Simonetti, L. Giraudet, T. Maurel, J.-L. Nicolas, and A. Belkhir, *Org. Electronics* **11**, 1381 (2010).

[21] F. Torricelli, Z. M. Kovcs-Vajna, and L. Colalongo, *Appl. Phys. Lett. 92*, 113306 (2008).

[22] F. Torricelli, Z. M. Kovcs-Vajna, and L. Colalongo, *IEEE Trans. Electr. Devices* **56**, 20 (2009).

[23] K.-D. Jung, Y. C. Kim, H. Shin, B.-G. Park, J. D. Lee, E. S. Cho, and S. J. Kwon, *Appl. Phys. Lett.* **96**, 103305 (2010).

[24] N. Kawasaki, Y. Ohta, Y. Kubozono, and A. Fujiwara, *Appl. Phys. Lett.* **91**, 123518 (2007).

[25] C.-L. Fan, Y.-Z. Lin, Y.-Y. Lin, and S.-C. Chen, *Org. Electron.* **14**, 3147 (2013).

[26] F. Torricelli, E. Cantatore, G. H. Gelinck, K. Myny, and J. Genoe, *13th Workshop on Semiconductor Advances for Future Electronics*, Veldhoven (The Netherlands), 170-174 (2010).

[27] F. Torricelli, K. ONeill, G. H. Gelinck, K. Myny, J. Genoe, and E. Cantatore, *IEEE Trans. Electr. Devices* **59**, 1520 (2012).

[28] B.H. Hamadani, D. Natelson, *J. Appl. Phys.* **97**, 064508 (2005).

[29] F. Torricelli, E. C. P. Smits, J. R. Meijboom, A. K. Tripathi, G. H. Gelinck, L. Colalongo, Z. M. Kovcs-Vajna, D. M. de Leeuw, and E. Cantatore, *IEEE Trans. Electr. Devices* **58**, 3025 (2011).